

ORIGINAL ARTICLE

Open Access

Polarizing cytoskeletal tension to induce leader cell formation during collective cell migration

Sebastian Rausch^{1,2}, Tamal Das^{1,2}, Jérôme RD Soigné^{4,5}, Tobias W Hofmann^{1,2}, Christian HJ Boehm^{1,2}, Ulrich S Schwarz^{4,5}, Heike Boehm^{1,2,3*} and Joachim P Spatz^{1,2}

Abstract

The collective migration of cells is fundamental to epithelial biology. One of the hallmarks of collective behavior in migrating cohesive epithelial cell sheets is the emergence of so called leader cells. These cells exhibit a distinct morphology with a large and highly active lamellipodium. Although it is generally accepted that they play a crucial part in collective migration, the biophysical factors that regulate their formation remain unknown. Here we show that a geometry-based cue like local variation of curvature of the collective's perimeter is capable of triggering leader cell formation and promoting enhanced motility at defined positions. Remarkably, the extent of this effect scales with the magnitude of the curvature.

Cytoskeletal tension was found to be important for geometry induced leader cell formation, as cells treated with tension reducing agents appeared less sensitive to local curvature variation. Accordingly, traction force microscopy revealed an increased level of shear stress at highly curved positions even before the cell migration had actually started, indicating the presence of a collective polarization induced by the geometry of the confinement.

Together our findings suggest that high curvature leads to locally increased stress accumulation, mediated via cell-substrate interaction as well as via cytoskeleton tension. The stress accumulation in turn enhances the probability of leader cell formation as well as cell motility. This work defines the importance of geometric cue such as local curvature in the collective migration dynamics of epithelial cells and thus shows implications for the biophysical regulation of epithelium during wound healing, embryonic development, and oncogenesis.

Keywords: Collective migration; Leader cell; Geometric constraint; Traction force; MDCK cells

Background

The collective migration of cells is an essential part of many important biological processes including morphogenesis [1], tumor invasion [2], and tissue repair [3].

A hallmark of collective migration is the appearance of so called leader cells. These cells exhibit a distinct morphology with a large and highly active lamellipodium [4]. In a classical wound-healing scenario these cells emerge at the leading edge of the migrating cell ensemble, where a fraction of cells acquires the leader cell characteristics early in the migration process [4,5].

Leader cells have been suggested to play an active role in guiding the collective forward [6-9] accompanied by

high tension within the collective [10]. As numerous cells behind the leading edge add considerably to the total traction force exerted on the substrate, leader cells might also merely happen to be in the leading position without adding a substantial share to the migration process [11,12]. Yet, leader cell formation has been consistently observed in collective cell migration, and thus it is generally accepted that leader cells play a crucial part in the migration process. Although their origin is assumed to be governed by a variety of chemical and physical signals, the basic biophysical factors underlying leader cell generation could not be conclusively identified [13].

In order to probe the role of the diverse and often conflicting signals, several recent studies have aimed at reducing the complexity of this multiparametric problem by creating well-defined model systems. In order to control the size and shape of cell ensembles, a very successful system has emerged making use of confinements of

* Correspondence: heike.boehm@is.mpg.de

¹Department of New Materials and Biosystems, Max Planck Institute for Intelligent Systems, Heisenbergstr. 3, 70569 Stuttgart, Germany

²Department of Biophysical Chemistry, University of Heidelberg, Im Neuenheimer Feld 253, 69120 Heidelberg, Germany

Full list of author information is available at the end of the article

different kinds [4,14-17]. This enables quantitative studies by reducing the complexity of the cell collective system by allowing the control of pivotal parameters of cell collectives, namely size, cell density and general shape [18]. Shape is described best by length and curvature of the cell collective's perimeter. As a matter of fact, controlling merely the parameter of curvature has been shown to reproduce experimental behavior of finger formation typically involved in leader cell formation in a computational model [19].

Moreover, several experimental studies indicate that the probability of leader cell formation might be enhanced by convex boundaries of the cell collective [20,21] similar to what has been shown for the directed migration of single cells [22]. Additional results highlighting the role of geometry for diverse physiological processes have been derived from experiments with spatially confined cell clusters. Cell collectives patterned on adhesive islands preferentially extended new lamellipodia from their corners [23]. Also, a strong correlation of geometry and cell proliferation was observed, revealing that the latter can be an active regulator of tissue growth [18]. Taken together, these findings hint towards curvature being a general parameter underlying biological and especially migration processes.

The question how local curvature in a confined setting affects leader cell formation in a subsequently triggered collective cell migration has not yet been resolved. We aim for a conclusive understanding of this crucial parameter and the underlying mechanisms involved. For this purpose we designed experiments that enabled us to largely emphasize local curvature as a mechanical cue in comparison to other factors. Therefore we developed a novel micro-stencil technique in order to precisely control the cell collective's area and its global as well as local perimeter curvature. We used two dimensional epithelial cell sheets on fibronectin coated surfaces in order to uncouple and analyze this particular parameter in a very well defined experimental setting. This allowed us to gain quantitative data by focusing on the role of curvature of the cell collective's perimeter on leader cell formation.

This work shows that local variation in curvature of the cell collective's perimeter correlates with locally increased motility, leader cell formation and traction stress. We identified the organization of the actin cytoskeleton and its collective polarization as a possible candidate for relying information about physical stress accumulation which in turn increases the probability of leader cell formation.

Methods

To obtain geometrically well-defined cell collectives, we employed micro-stencils made of polydimethylsiloxane (PDMS). Stencil masks were fabricated in an adapted

soft lithography process [24]. In short, SU-8 25 negative photo resist (MicroChem, Newton, MA, USA) was spin-coated on a 2" silicon wafer (Si-Mat, Kaufering, Germany) in a clean room facility, prebaked on a hot plate, illuminated for 12 sec in Mask Aligner MJB4 (Suess MicroTec Lithography, Munich, Germany) and baked again on a hot plate. To remove non-irradiated SU8 resist, wafers were bathed in SU-8 Developer mr-Dev600 (Microresist Technology, Berlin, Germany) and then treated with 1H,1H,2H,2H-Perfluorooctyl-trichlorosilane to reduce adhesiveness. A sandwich consisting of the wafer with photoresist structures, 0.5 mL of uncured PDMS, a piece of parafilm, a piece of paper and a glass slide was put into a custom made molding press to obtain uniform pressure distribution. The assembly was put into a compartment dryer at 65°C for 100 min to allow PDMS polymerization. PDMS membrane thickness of 50–60 μm was achieved regularly. To prevent cell adhesion, stencil masks were incubated in a solution of Pluronic F-127 (Sigma Aldrich, 2% w/v in deionized water) for 30 minutes prior to use.

MDCK II cells were seeded on fibronectin coated surfaces partially blocked by micro-stencils. They were maintained in Minimum Essential Medium Eagle supplemented with 5% FBS, 2 mM L-glutamine, 10U mL^{-1} penicillin and 10 $\mu\text{g mL}^{-1}$ streptomycin. The average density of cells compromising a single collective was about 3600 cells/ mm^2 , or 350 cells per collective.

Time lapse image acquisition was performed on an inverted Observer microscope (Zeiss, Germany) directly after removal of the micro-stencils. Phase contrast images of at least 95 individual collectives distributed into at least two independent experiments for each stencil type used were acquired every 5 min using a 10x objective. Coordinates and timepoints of leader cell formation were determined by hand. All other data analysis were performed with Matlab (Mathworks, Germany).

Inhibition experiments were conducted with Blebbistatin and Y-27632 to reduce cytoskeleton tension. Drugs were added to the medium 1 hour before start of the experiment in a concentration of 50 μM (Blebbistatin) or 30 μM (Y-27632). During experiments, i.e. after removal of the stencil mask, cells were maintained in standard cell culture medium supplied with 5 μM blebbistatin or 3 μM Y-27632, respectively. For control experiments cell collectives were incubated for one hour in Opti-MEM containing DMSO (1 μL per mL of medium) before the stencil mask was removed. The experiment was then conducted in standard cell culture medium.

Traction force microscopy was carried out as previously described [25] on polyacrylamide (PAA) substrates with a Young's modulus of about 23kPa, in which fluorescent 500 nm carboxylated polystyrene beads were embedded as position markers. To ensure cell attachment PAA was covalently functionalized with fibronectin.

Bead displacements were tracked following a Matlab adaptation of the algorithm developed by Crocker and Grier [26]. Subsequently a regularized Fourier-transform traction cytometry was employed to calculate the traction [27] in each independent cell collective of which 17 were superimposed to calculate the average stress distribution. For all traction field reconstructions the regularization parameter, which effectively filters out high frequency noise, was kept constant.

Cell stainings were performed on fixed and permeabilized cells with the primary antibody, rabbit monoclonal [clone Y113] to Paxillin (ab32084, Abcam, Germany), followed by anti-rabbit secondary antibody tagged with the fluorescent dye Alexa Fluor 488 (Invitrogen, Germany), and with DNA-binding dye 4',6-diamidino-2-phenylindole (DAPI, 1 $\mu\text{g}/\text{ml}$ in PBS, Invitrogen, Germany). Visualization of the actin cytoskeleton was done by adding TRITC-labeled phalloidin at the secondary incubation step, if required.

Analysis of the actin belt was based on the computation of the angular distribution of stained actin within an approximately 4 μm wide region along the boundary of the cell collectives.

The significance in all experiments was determined using the Mann–Whitney–Wilcoxon test.

Contraction of the colony monolayer was simulated using a two-dimensional continuum model that has been introduced previously by Edwards and Schwarz [28]. In this model, an isotropic and homogeneous active stress is introduced into the elastic equations for a thin elastic sheet which in turn is coupled to an elastic foundation. For a given geometry, this model is solved numerically with Finite Element Methods (FEM) in Comsol Multiphysics. The model has two free parameters, the coupling constant κ and the contractile pressure σ_{con} . As input for the model fitting we used the derived mean displacement field and reconstructed traction pattern. From the model the traction can be calculated by $T = \kappa u$, while u is the calculated model displacement, which depends on both σ_{con} and κ . The parameters were optimized by sampling, fitting once the data of the spike shaped pattern. Here, we adjusted the parameters in such a way that a best agreement with measured displacement and reconstructed traction pattern was achieved. More details on the methods described in this section can be found in the supplementary information (Additional file 1).

Results and discussion

Migration assay of geometrically well defined epithelial cell collectives

We sought to derive quantitative information on the influence of curvature on collective cell migration driven by the formation of leader cells. For this purpose we developed a micro-stencil technique to reproducibly create cell collectives with well-defined geometrical shapes.

The essential part of the micro-stencils is a thin PDMS-membrane with precisely defined holes that can be placed on any adhesive surface. Initially the cells form a monolayer covering the area inside the holes in the geometry induced by the PDMS stencil. Removal of the stencil triggers free migration of cells on the freshly uncovered substrate. Since cells are not damaged in this process, the experimental conditions are better controlled in comparison to classical scratch wounding assays, where local necrotic damage might influence cell behavior.

To generate cell collectives with varying local curvature, we created three different stencil masks in this study (Figure 1A). All three are based on a circle with a diameter of 350 μm . First we created masks to form perfectly circular cell collectives containing approximately 350 Madin-Darby canine kidney (MDCK II) epithelial cells. On two other sets of masks, four small protrusions are added to enhance the local curvature at four positions. We created collectives with protrusions of hemispherical shape with a radius of 35 μm increasing the local curvature five fold at the protrusions in comparison to the rest of the collective's perimeter. These small protrusions with an area of 2000 μm^2 correspond to an average of 6 cells. Finally we created collectives with very high local curvature by employing triangular protrusions of the same area, with a base length of 60 μm and a height of 67 μm .

The geometry induced by the stencil boundary was reproduced perfectly in all cases by the cell collectives upon reaching confluency (Figure 1B). In course of the experiment, the removal of the stencil mask opened up the free substrate space without damaging the cells. This action was sufficient to trigger migration of the cell collectives without the need to apply any other means of stimulation, like e.g. growth factors (Figure 2, see also Additional file 2: Movie S2).

In order to assess the influence of local curvature on the onset of collective migration, we first studied at which positions of the perimeter the formation of leader cells took place. It is understood that their appearance is robust and a direct marker for the onset of collective migration processes [29-31]. By analyzing time lapse image series we could pinpoint the exact time and place of leader cell formation. We defined leader cells as cells at the perimeter that developed a large lamellipodium and were actively involved in the radial outward migration process at the tip of a multicellular outgrowth. Only cells that maintained their active behavior at the tip of the finger for at least two hours were taken into account. We first analyzed collectives of perfectly circular shape, which offered an isotropic reference system without any preferred spatial direction. Due to the rotational symmetry, we assigned each position of leader cell appearance an angle relative to an arbitrarily

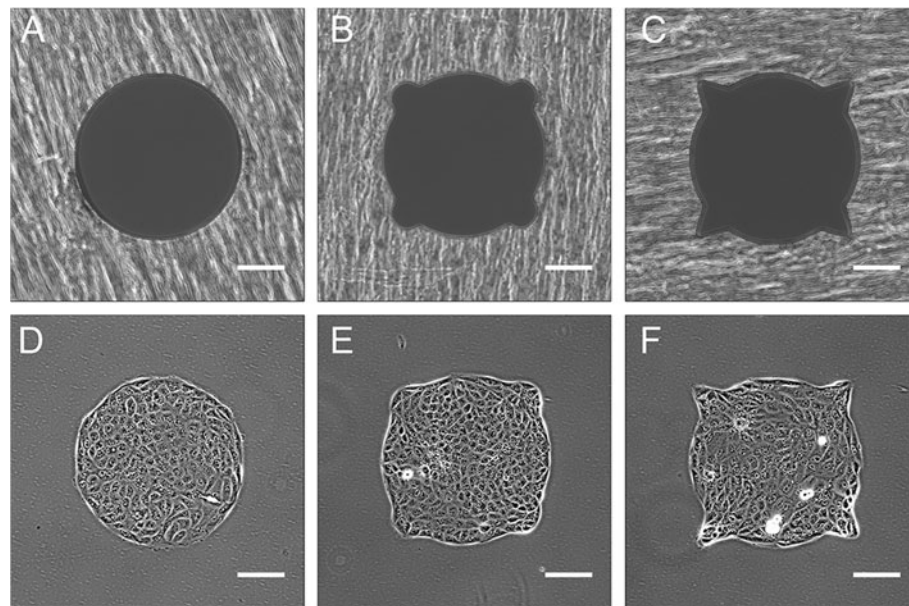


Figure 1 Generation of cell collectives with defined geometry. Microscopy images of stencil-masks (A to C) and cell collectives reproducing the given motif after the stencil has been removed: (D) circular (E) with medium curvature and (F) with high curvature. Scale bars correspond to 100 μm .

fixed direction. In this collective geometry we found that the positions of leader cell formation showed a completely homogeneous distribution over the whole range of 360° (Figure 3A, averaged data consolidated into one quadrant). The appearance of new leader cells occurred throughout the whole experimental timeframe, a fraction of leader cells still appeared several hours after the onset of migration. Nevertheless, more than half of them formed during the first 90 minutes after the physical barrier was lifted (Additional file 3: Figure S3).

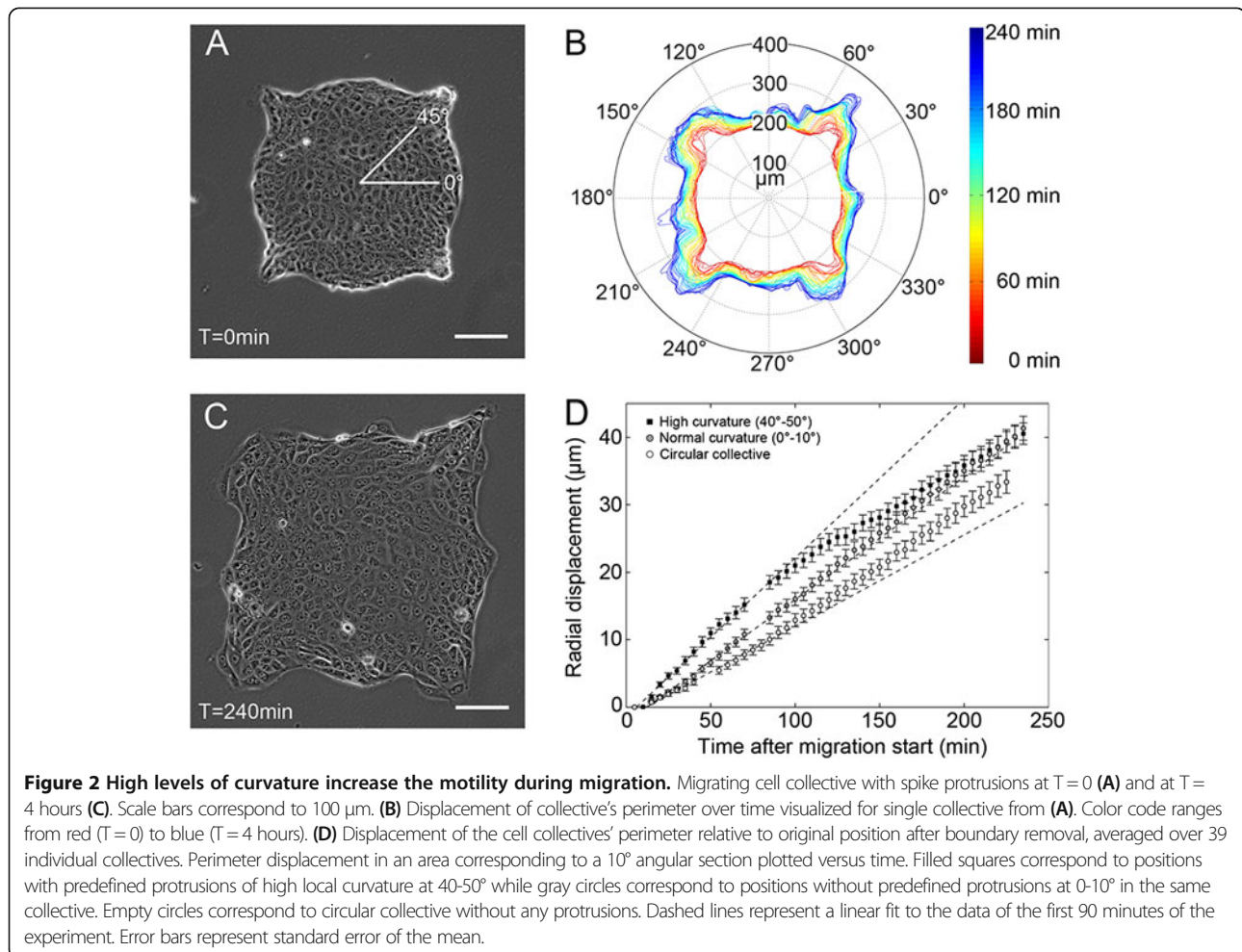
Next we investigated if the increase in local curvature using collective geometry with hemispherical protrusions alters the behavior of the collective. Again we analyzed the angular position of leader cell appearance, this time in such a way that the center of the protrusions was located at an angle of 45° to an arbitrarily fixed line. We observed an enhanced probability of leader cell formation at the angles corresponding to the positions of hemispherical protrusions (Figure 3B). Interestingly, the formation of leader cells in this case was also slightly delayed on average. There were still leader cells forming at every time point of the experiment, but only one third of the total number formed during the first 90 minutes (Additional file 4: Figure S4).

Finally, we used collective geometry with triangular protrusions, which introduced an even higher local curvature into the system at the tip of the triangle. We found that in this setting, the probability of leader cells forming at the protrusions is again increased almost twofold with respect to the hemispherical design (Figure 3C). This increase can directly be attributed to

the higher local curvature, since the only difference to the former setting is the different geometry yielding an increased curvature at the tip of the triangle. In this scenario more than half of the leader cells formed during the first 90 minutes of the experiment (Additional file 5: Figure S5).

The average number of leader cells forming over 6 hours per collective was determined to be 10.0 ± 0.2 for circular collectives, 8.5 ± 0.2 for collectives with hemispherical protrusions and 10.4 ± 0.2 for collectives with spike protrusions. This shows that not all of the leader cells were emerging at one of the protrusions. However, we intentionally placed the protrusions at low proximity in order to have them separated spatially far enough as to avoid interference between them. Yet, these results clearly show that the actual position of leader cell appearance changes from a random distribution towards a distribution with enhanced probability at positions of higher local curvature and that this effect scales with the magnitude of the local curvature.

Furthermore, we analyzed the displacement speed of the collective's perimeter over time. In addition to the earlier observation of increased probability for leader cell formation at spike protrusions, we also observed that the radial velocity of migration of the perimeter at these positions is higher during the early stage of migration (i.e. during first two hours of migration, Figure 2D). A linear fit to the data of the first 90 minutes shows an average velocity at the spike protrusions of $0.24 \mu\text{m min}^{-1}$ (filled quares in Figure 2D) which is significantly higher than the average velocity of $0.18 \mu\text{m min}^{-1}$ (gray circles



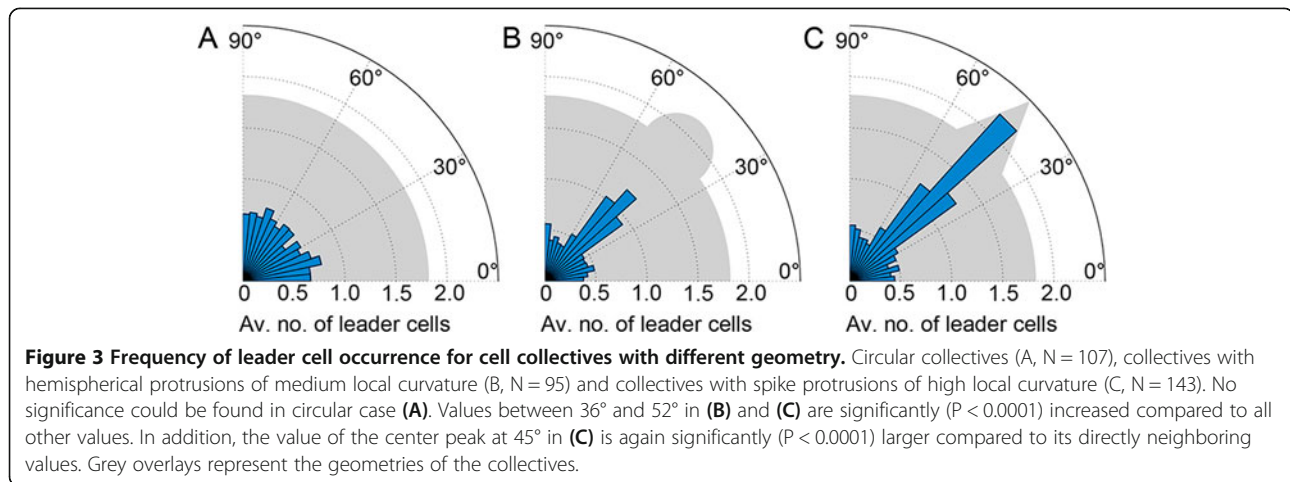
in Figure 2D) at the normal curved regions. The local increase in velocity correlates directly with the enhanced formation of leader cells at these positions indicating that they indeed play an important role for the migration process by locally enhancing the outward directed migration speed. A fit to the data of perimeter displacement of a completely circular collective without protrusions of enhanced curvature yielded an average cluster expansion velocity of only $0.14 \mu\text{m min}^{-1}$ (white circles in Figure 2D). This velocity of $0.14 \mu\text{m min}^{-1}$ at collectives without protrusions is slower than the velocity of $0.18 \mu\text{m min}^{-1}$ within the 0° to 10° angular section of collectives with protrusions, although the local curvatures are identical in these both cases. Thus, the increase in curvature not only increases the velocity at positions of high local curvature, but also leads to a general velocity increase across the whole collective even at positions without increased curvature.

Taken together our results show a clear correlation between increased probability of leader cell formation and increased local curvature resulting in turn in a locally enhanced migration velocity of the cell collective. Thus,

leader cell formation in fact plays an active role in the collective migration process.

Role of intracellular tension in geometry induced leader cell formation

Previous studies indicate that cell monolayers exist in a state of tensile stress [11,32,33]. Additionally, it has been shown that extracellular compressive stress such as one imposed by the hydrostatic pressure plays a role in leader cell formation [21]. This observation led us to the question if an increase in local perimeter curvature is actually accompanied by an increased local tension or stress level as a reaction of the cell collective. To test this hypothesis, we treated cell collectives with blebbistatin and Y-27632 which are known to reduce the intracellular tension. Blebbistatin inhibits myosin II activity [34] and thus cell motility. The pyridine derivative Y-27632 is known to inhibit the Rho-associated protein kinase (p160ROCK) pathway, which in turn directly decreases actomyosin-mediated contractile tension [35]. We used these drugs in concentrations that have recently been shown to not compromise the stress induced leader cell formation [21].



We incubated cell collectives with blebbistatin or Y-27632 and again analyzed the angular distribution of leader cell emergence at the cell collectives' perimeters. We found that their appearance was no longer favored to the angular range of the protrusions but they tended to emerge randomly along the collectives perimeter. Only a small fraction was still showing up at the positions of the protrusions. In comparison to non-treated collectives the percentage of leader cells appearing at the positions of spike protrusions was reduced significantly by a factor of two. Within experimental accuracy, this effect was identical for both drugs used (Figure 4B and C). In both cases the drugs diminished the influence of the present protrusions with higher local curvature.

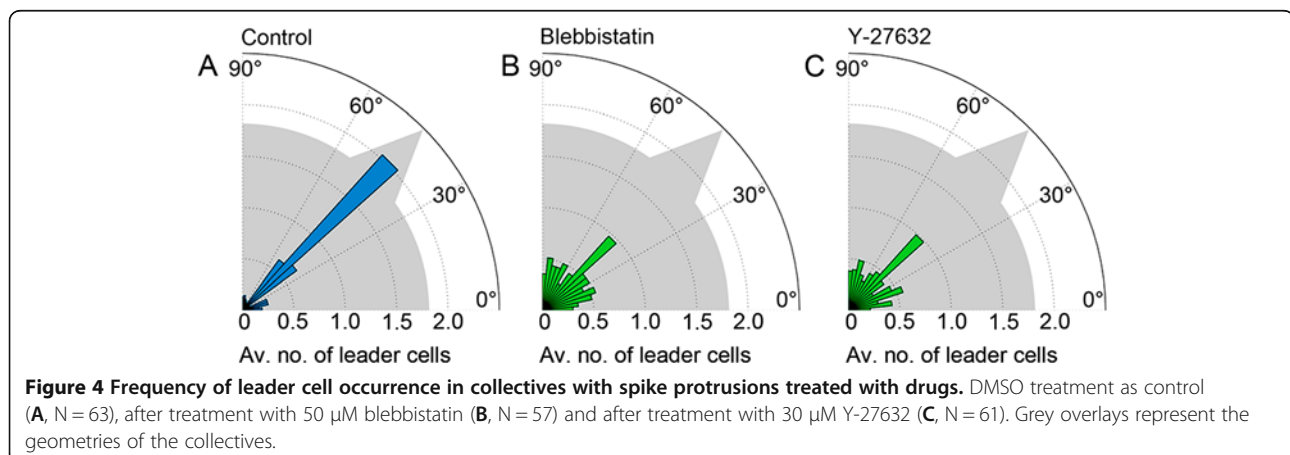
The addition of DMSO as a vehicle for both drugs was shown not to influence the experimental conditions in an independent set of control experiments (Figure 4A).

In conclusion these results offer complementary data to our previous finding that the probability of leader cell formation scales with the intracellular tension. A slightly enhanced probability still remains at the highly curved regions even after drug treatment. Nonetheless, the

magnitude of the effect clearly shows that in fact cytoskeletal tension plays an important role in the formation of leader cells.

Curvature dependent increase in local traction force at the cell-substrate interface

To further investigate the role of intracellular stress on the formation of leader cells we employed traction force microscopy. This technique allows us to gain direct insight on mechanical cell-substrate interactions. We used a well-established protocol [25] going back to the original work of Pelham and Wang [36] based on a polyacrylamide gel substrate with fluorescent microbeads embedded as position markers. Upon migration of the cells on this substrate the microbeads are displaced due to the traction stress exerted on the gel by the cells. The traction exerted on the substrate can be calculated from the displacement fields of the microbeads using regularized Fourier-transform traction cytometry [27], a refinement of a previously introduced method [37]. With this technique quantitative data on the distribution of traction stress exerted by the cells can be obtained with high



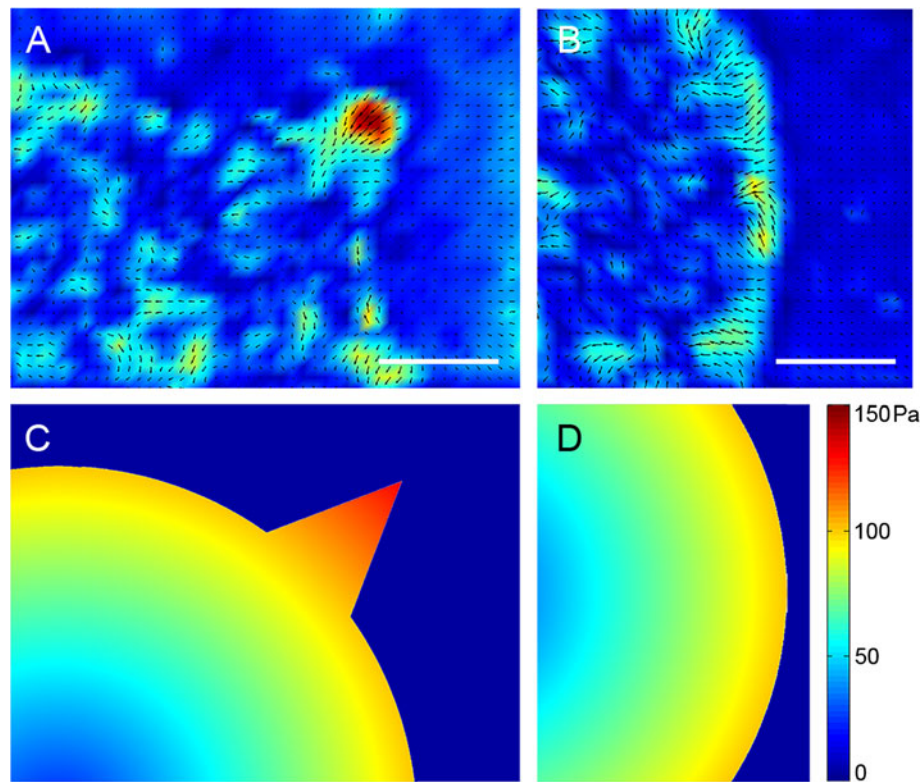


Figure 5 Averaged traction force data and numerical model of corresponding geometry. By superimposing the vectorial stress fields of multiple traction force microscopy measurements, an averaged stress field could be acquired that highlights similarities between individual measurements. For better visualization the average magnitudes of these stress fields are shown in color-coded images for high local curvature (A, N = 17) and normal curvature (B, N = 17). Scale bars correspond to 50 μm . Results from numerical simulations are shown in (C) and (D), for high local curvature and normal curvature, respectively. The model explains the high stress localization in the highly curved protrusions and the increased traction level homogeneously distributed along the collective's perimeter at the normal curved perimeter.

spatial resolution (see also Additional file 6: Figure S6). By acquiring data directly after removal of the stencil mask we could assess the traction stress distribution before the appearance of leader cells which did not emerge until 15 minutes later in the experiment. For this

purpose we acquired data at two different positions of the collective, namely at the position of a spike protrusion and at the normal curved perimeter. We obtained the traction stress distribution for each individual image and then averaged the data on the level of force vectors

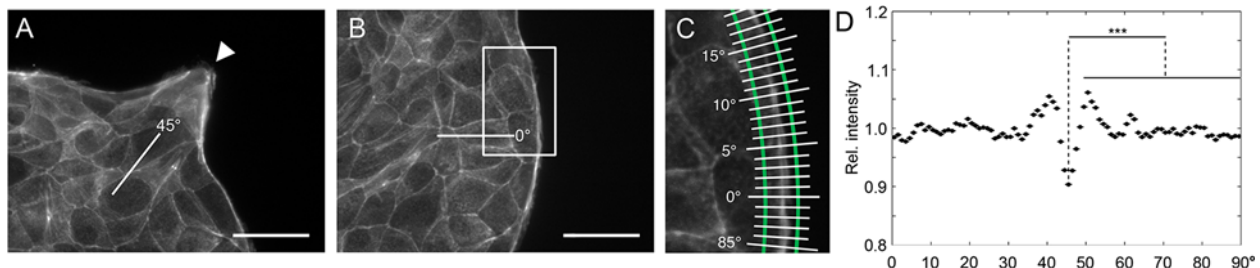


Figure 6 Phalloidin staining of multicellular actin structure directly after stencil mask removal. At the position of a highly curved protrusion (A) and at a normal curved perimeter (B). A multicellular actin structure lining the whole perimeter can be seen in B while at the tip of the highly curved protrusion in A a distinct opening in the actin fibers can be observed as indicated by the arrow. Intensity analysis was done in a stripe of 4 μm along the perimeter as seen in (C, magnification of the area of 45 \times 68 μm marked in B). The mean fluorescence intensity levels along the perimeter of the collectives with highly curved protrusions are shown in D. Individual quadrants of the perimeter were registered and averaged. At an angle of 45°, corresponding to the highly curved position, a significant dip in intensity is present ($P < 0,0001$ compared to the relative intensities at angles ranging from 48° to 90°, as well as 0° to 42°). Error bars denote standard error of the mean, N = 432. Scale bars correspond to 50 μm .

by superimposing the results of 17 collectives. Thus, we attained the average characteristics of the cell collective, independent of the details of the individual experiments. We thus determined whether there are fundamental similarities present in all of the collectives. In order to visualize the results, color coded maps were created that show the mean spatial distribution of traction stress magnitudes (Figure 5). This traction force landscape shows a roughened background in the bulk of the collective which stems from the different individual states each of the collectives was in during data acquisition. Despite this average roughness, there are no localized accumulations of stress present in the bulk. However, in the vicinity of the tip of the highly curved protrusion a prominent accumulation of traction force is present. At this clearly distinguishable hot spot cells generate a stress field of high magnitude directed towards the bulk of the collective (Figure 5A). In contrast, at the normal curved perimeter an increased level of traction force is present, but in this case it is continuously distributed along the perimeter with no distinct force localization (Figure 5B). Here also the stress is directed radially towards the bulk, reflecting the general tendency of the collective to migrate into open space. This observation is in agreement with the recent description of kenotaxis [33].

This evidence shows that cells within the protrusions with high local curvature exert strong pulling forces on the substrate even before onset of the outward directed migration process. In contrast, there is no such pronounced accumulation of traction stress present near or at the normal curved perimeter, ruling out the possibility that this effect is simply due to the proximity to the collective's perimeter itself.

Since much of the cellular traction is known to be transmitted through sites of focal adhesion, we further looked into the distribution and orientation of focal adhesion points at different locations of the collectives. Focal adhesions play a major role in connecting cells with the substrate in order to exert forces, and they are involved in transmitting mechanical forces as well as regulatory signals. We stained cell collectives with antibodies against the focal adhesion complex protein Paxillin to gain further information on the mechanical stress state between cells and substrate. The necessary fixation was done directly after removal of the stencil mask, allowing no time for major reorganization of focal adhesions which takes at least several minutes [38]. At the cell collectives perimeter we found a striking difference in the orientation of focal adhesion points between areas of normal curvature and areas of protrusions with high curvature. The focal adhesions in the normal curved regions are oriented tangential to the perimeter of the collective. In contrast, the focal adhesions in the area of a spike protrusion are oriented radially with

respect to the center of the collective (Additional file 7: Figure S7). This correlates well to the results of the traction force microscopy experiments.

We further investigated the relevance of local curvature for the appearing stress distribution within the collective using a two-dimensional continuum model which has been introduced previously by Edwards and Schwarz [28]. Here, the cell collective was represented by a homogeneous contractile layer of an elastic, isotropic material which is elastically coupled to the substrate. This represents the fact that contractile forces are generated and transmitted throughout the entire cell monolayer while each individual cell feels its interaction with the underlying substrate locally. The two free model parameters colony contractility σ_{con} and the substrate coupling constant κ have been fitted regarding only the two values for maximal measured mean displacement and traction of all experiments as well as their respective geometry (Figure 5C). As values we derived $\kappa = 130 pN/\mu m$ and $\sigma_{con} = 3.8 pN/\mu m$. Although the model represents a coarse-grained situation, generic differences in traction magnitude based on the initial geometry are clearly evident. The model predicts both the homogeneously distributed elevated traction at the rim and the pronounced stress distribution in the protrusions. In particular, it predicts a difference in the average stress distribution of about 50 Pa between the highly curved protrusion at 45° (Figure 5C) and the circular part at 0° (Figure 5D) in good agreement with the experimental results.

In summary these results show that the local increase in curvature is sensed by the cell collective and converted into a local accumulation of traction force at the cell-substrate interface. This change in cell induced stress distribution is also reflected by the reorientation of the focal adhesions which link the cytoskeleton to the substrate. When we analyzed this situation in a numerical continuum model, we found that contractile forces in conjunction with geometry are sufficient to explain the accumulation of traction stress in regions of high local curvature. This agreement clearly shows that regarding stress distribution, cells within the cell collectives act in a collective manner rather than as single cells.

Role of pluricellular actin belt for leader cell formation

Stress fibers consisting of actomyosin bundles play an important role for mechanotransduction in diverse cellular systems [39]. Enhanced mechanical stress levels in the cells favor the formation of stress fibers. Since our results from traction force microscopy strongly indicate that local accumulation of traction stress favors the formation of leader cells, we decided to look into the distribution of actin filaments in more detail.

In multicellular systems, connected actin cytoskeletons transmit intercellular stress over length scales larger than

a single cell [10]. A multicellular actin belt, comprised of actin stress fibers lining the perimeter of cell collectives, has been reported previously in many *in vivo* and *in vitro* systems [40,41]. This structure plays a major role in the purse string wound closure and in multicellular migration [4,5,7]. The purse string model describes wound healing of mainly small wounds with concave boundaries by formation of an actomyosin cable and subsequent contraction of the actin belt at the wound borders. It is believed that the actin bundles (also called actin cables) play a role for force transmission to distribute arising forces more evenly among cells of differing activity [12].

When we stained the actin in cell collectives grown to confluency within a micro stencil with spike protrusions, we found an encompassing multicellular subcortical actin belt at the cell collective's perimeter. Although within the collective single cell bodies could clearly be identified by their cytoskeleton, an affiliation of parts of the belt structure to individual cells was not possible anymore. Interestingly, we observed that this actin structure had been assembled prior to the onset of migration, i.e. before removal of the stencil mask. We observed this pluricellular actin structure over the length of the surrounding convex boundaries of the multicellular collectives. Intriguingly at the very tip of the spike protrusions we found a diminished amount of actin fibers. At these positions the actin belt was present not at all or at least only very weakly (Figure 6A) compared to the normal curved boundary (Figure 6B). In order to gain a quantitative measure for this observation we determined the relative fluorescence intensity along the perimeter of each collective corresponding to the actin belt (Figure 6C, see also Additional file 8: Figure S8). The data derived here clearly shows a significant dip in intensity around 45° ($P < 0.0001$ compared to the relative intensity at 0°) which directly corresponds to the tip of the highly curved spike protrusions (Figure 6D, $N = 432$).

In contrast to the purse string model, which is assumed for small concave wounds, our observation is based on structures with convex boundaries. However, in the experiments presented here the actin belt might also be involved in force transmission, similar to a purse string model where contractile stress is mediated by actomyosin bundles. The break in the actin belt structure at the very tip of the highly curved spike protrusions is formed before the barrier is lifted, i.e. before migration starts. It is reasonable to assume that this might facilitate the outgrowth of cells in the subsequent migration process, and thus result in higher incidences of leader cell formation.

Conclusion

In order to study the collective behavior of migrating epithelial cell sheets, we designed PDMS-membranes that induce well-controlled geometrical constraints on the cell collectives. Thus we were able to compare the effect of

different local curvatures of the perimeter on the collective's migration behavior. The evidence described here clearly shows that the collective is polarized in terms of mechanical stress even before the onset of the migration process. This stress polarization is directly translated to an increased probability of leader cell formation and thus higher migration velocity. This is evident by a break in the actin belt, the inhomogeneous force distribution map, as well as the orientation of focal contacts and is further supported by complementary data from a mathematical model.

The distribution of actin stress fibers is known to give insights into the state of tension in cells. We observed a prominent pluricellular actin belt encompassing the whole collective. These actin bundles might give a possible explanation on how cells transmit curvature information over many cell lengths. Since they span the whole cell collective's perimeter they might be in a tensile state resembling the local curvature situation. The mechanotransducing effect of these bundles might thus gather strain information and transmit it to the tip point where the curvature and thus local strain is too high to maintain the structural integrity. Accordingly, at these tips we observed a gap in the actin rich structure giving the tip cells an advantage during the onset of migration. They are thus more prone to become leader cells due to less obstructive force of the actin bundles.

Similarly, the traction stress distribution is sensitive to the geometry of the collective. The accumulation of traction stress shows that these cells undergo what we call stress polarization. Here, we discovered a considerable accumulation of stress pointing towards the center of the collective in sections of the perimeter with high local curvature. This is further supported by the finding that focal adhesions in highly curved protrusions are oriented radially.

The initial collective polarization might give cells at the positions of high local curvature a head start when the migration process is initiated by removal of the physical barrier. This explains the increased migration velocity and the significantly enhanced probability of leader cell formation at highly curved protrusions in comparison to perimeters with lower local curvature. The increased probability of leader cell formation scales with the magnitude of the curvature increase and is consistent with our finding that by inhibiting cytoskeletal tension through the addition of drugs the angular distribution of leader cell formation is broadened drastically. In this case the information that a portion of the collective is exposed to higher tension due to curvature can no longer be transmitted sufficiently enough between cells and the prepolarizing effect is mostly lost.

In general, woundhealing scenarios can roughly be divided into two major categories depending on the wound size. One is the closure of very small wounds, which has been shown to take place by an actively contracting

actomyosin cable at the wound perimeter [40]. The other mechanism, which can be observed at larger wounds, is the active collective migration of cells towards each other for a reepithelialization of the denuded wound surface [4]. Our results suggest that in our experimental framework both mechanisms contribute to a collective migration scenario: The active migration of monolayers of cells in response to increased magnitudes of curvature is supported by a multicellular actin structure playing a role in information transmission before the actual active migration takes place.

It is reasonable to assume that in an *in vivo* situation the reaction to local curvature is also beneficial for invading tumor cell clusters. There, a small local difference in the rigidity of the surrounding tissue might easily lead to a formation of a locally slightly higher curved region in the tumor surface area. This in turn enhances migrational activity towards the weaker part of the surrounding tissue.

Our results show that plain geometrical parameters, in this case curvature variation, have a major impact on collective cell migration in spite of the inherent complexity of the living system.

Additional files

Additional file 1: Supporting Information.

Additional file 2: Movie S2. Migrating cell collective with highly curved protrusions. First image was acquired directly after removal of the physical barrier. Image acquisition rate was five minutes per frame over a total time of four hours. Scale bar corresponds to 100 μm .

Additional file 3: Figure S3. Leader cell development over time for circular collectives. The angular distribution of leader cell formation is shown for different time intervals, (A) 0–90 min, (B) 91–180 min, (C) 181–270 min and (D) 271–360 min, respectively. Data has been averaged for $N = 107$ individual collectives and consolidated into a single quadrant.

Additional file 4: Figure S4. Leader cell development over time for collectives with hemispherical protrusions of medium local curvature. The angular distribution of leader cell formation is shown for different time intervals, (A) 0–90 min, (B) 91–180 min, (C) 181–270 min and (D) 271–360 min, respectively. Data has been averaged for $N = 95$ individual collectives and consolidated into a single quadrant.

Additional file 5: Figure S5. Leader cell development over time for collectives with spike protrusions of high local curvature. The angular distribution of leader cell formation is shown for different time intervals, (A) 0–90 min, (B) 91–180 min, (C) 181–270 min and (D) 271–360 min, respectively. Data has been averaged for $N = 143$ individual collectives and consolidated into a single quadrant.

Additional file 6: Figure S6. Representative example of data analysis procedure via traction force microscopy. After simultaneous acquisition of a phase contrast image and a fluorescent image of embedded microspheres (A) the beads' displacement field was calculated relative to a reference image taken without cells present (B). Regularized Fourier-transform traction cytometry was subsequently used to derive the stress field (C). Scale bars correspond to 50 μm .

Additional file 7: Figure S7. Curvature dependence of focal adhesion orientation. Overlay of fluorescence microscopy images of an antibody staining for vinculin (red) and actin (green) at normal curved region (A) and at highly curved region (C). Inverted images of the vinculin staining are shown for clarity in (B) and (D), respectively. Orientations of focal

adhesions at the perimeter are tangential in normal curved regions (B) and radial in highly curved regions (D). Scale bars correspond to 50 μm .

Additional file 8: Figure S8. Evaluation procedure of actin rich structures at the perimeter of cell collectives. (A): Automatically generated overlay of the fluorescence micrograph of a cell collective and control markers. The quadrants selected for analysis are labeled with green filled circles and those which were discarded with red crosses. The contour of the boundary region of the collective is marked in green. The blue circle was fitted to the collective's shape to determine its center. (B) Mask of a cell collective rotated by an angle $\alpha = 5^\circ$ with respect to the horizontal showing the polar coordinates used for each quadrant. (C) Angular distribution of the mean normalized intensities in the boundary regions of the analyzed cell collectives (red), and for a control collective of homogeneous intensity (blue). Error bars are standard errors of the mean. Scale bars correspond to 100 μm .

Competing interests

The authors declared that they have no competing interests.

Authors' contributions

SR, CHJB, HB and JPS designed research, SR and TD performed research, SR, TWH, HB analyzed data, JS and USS analyzed traction force data and performed modeling, SR, TD, HB and JPS wrote the paper. All authors read and approved the final manuscript.

Acknowledgments

The authors thank Christiane Antoni for technical assistance and Tabea Munding for proof reading and valuable discussion. This work was supported by the Max-Planck Society. JPS is the Weston Visiting Professor at the Weizmann Institute of Science. JPS and USS are members of the Heidelberg cluster of excellence CellNetworks. This work was supported by CellNetworks EcTop2, the grass-root project of the Max Planck Institute for Intelligent Systems, and the MechanoSys-grant of the BMBF. The funders had no role in study design, data collection and analysis, decision to publish, or preparation of the manuscript.

Author details

¹Department of New Materials and Biosystems, Max Planck Institute for Intelligent Systems, Heisenbergstr. 3, 70569 Stuttgart, Germany. ²Department of Biophysical Chemistry, University of Heidelberg, Im Neuenheimer Feld 253, 69120 Heidelberg, Germany. ³CSF Biomaterials and Cellular Biophysics, Max Planck Institute for Intelligent Systems, Heisenbergstr. 3, 70569 Stuttgart, Germany. ⁴University of Heidelberg, Bioquant, Im Neuenheimer Feld 267, 69120 Heidelberg, Germany. ⁵Institute for Theoretical Physics, University of Heidelberg, Philosophenweg 19, 69120 Heidelberg, Germany.

Received: 15 October 2013 Accepted: 12 November 2013

Published: 22 November 2013

References

1. Streichan SJ, Valentin G, Gilmour D, Hufnagel L (2011) Collective cell migration guided by dynamically maintained gradients. *Phys Biol* 8(4):045004
2. Friedl P, Hegerfeldt Y, Tusch M (2004) Collective cell migration in morphogenesis and cancer. *Int J Dev Biol* 48(5–6):441–449
3. Martin P (1997) Wound Healing—Aiming for Perfect Skin Regeneration. *Science* 276(5309):75–81
4. Poujade M, Grasland-Mongrain E, Hertzog A, Jouanneau J, Chavrier P, Ladoux B, Buguin A, Silberzan P (2007) Collective migration of an epithelial monolayer in response to a model wound. *Proc Natl Acad Sci* 104(41):15988–15993
5. Omelchenko T, Vasiliev JM, Gelfand IM, Feder HH, Bonder EM (2003) Rho-dependent formation of epithelial “leader” cells during wound healing. *Proc Natl Acad Sci* 100(19):10788–10793
6. Khalil AA, Friedl P (2010) Determinants of leader cells in collective cell migration. *Integr Biol* 2(11–12):568–574
7. Lim JI, Sabouri-Ghomi M, Machacek M, Waterman CM, Danuser G (2010) Protrusion and actin assembly are coupled to the organization of lamellar contractile structures. *Exp Cell Res* 316(13):2027–2041

8. Vitorino P, Meyer T (2008) Modular control of endothelial sheet migration. *Genes Dev* 22(23):3268–3281
9. Aigouy B, Lepelletier L, Giangrande A (2008) Glial chain migration requires pioneer cells. *J Neurosci* 28(45):11635–11641
10. Reffay M, Petitjean L, Coscoy S, Grasland-Mongrain E, Amblard F, Buguin A, Silberzan P (2011) Orientation and polarity in collectively migrating cell structures: statics and dynamics. *Biophys J* 100(11):2566–2575
11. Trepats X, Wasserman M, Angelini T, Millet E, Weitz D, Butler J, Fredberg J (2009) Physical forces during collective cell migration. *Nat Phys* 5(6):426–430
12. Farooqui R, Fenteany G (2005) Multiple rows of cells behind an epithelial wound edge extend cryptic lamellipodia to collectively drive cell-sheet movement. *J Cell Sci* 118(Pt 1):51–63
13. Trepats X, Fredberg JJ (2011) Plithotaxis and emergent dynamics in collective cellular migration. *Trends Cell Biol* 11(21):638–646
14. Vedula SRK, Leong MC, Lai TL, Hersen P, Kabla AJ, Lim CT, Ladoux B (2012) Emerging modes of collective cell migration induced by geometrical constraints. *Proc Natl Acad Sci* 109(32):12974–12979
15. Anon E, Serra-Picamal X, Hersen P, Gauthier NC, Sheetz MP, Trepats X, Ladoux B (2012) Cell crawling mediates collective cell migration to close undamaged epithelial gaps. *Proc Natl Acad Sci* 109(27):10891–10896
16. Ng MR, Besser A, Danuser G, Brugge JS (2012) Substrate stiffness regulates cadherin-dependent collective migration through myosin-II contractility. *J Cell Biol* 199(3):545–563
17. Hirashima T, Hosokawa Y, Lino T, Nagayama M (2013) On fundamental cellular processes for emergence of collective epithelial movement. *Biol Open* 2(7):660–666
18. Nelson CM, Jean RP, Tan JL, Liu WF, Sniadecki NJ, Spector AA, Chen CS (2005) Emergent patterns of growth controlled by multicellular form and mechanics. *Proc Natl Acad Sci* 102(33):11594–11599
19. Mark S, Shlomovitz R, Gov NS, Poujade M, Grasland-Mongrain E, Silberzan P (2010) Physical model of the dynamic instability in an expanding cell culture. *Biophys J* 98(3):361–370
20. Rolli CG, Nakayama H, Yamaguchi K, Spatz JP, Kemkemer R, Nakanishi J (2012) Switchable adhesive substrates: revealing geometry dependence in collective cell behavior. *Biomaterials* 33(8):2409–2418
21. Tse JM, Cheng G, Tyrrell JA, Wilcox-Adelman SA, Boucher Y, Jain RK, Munn LL (2012) Mechanical compression drives cancer cells toward invasive phenotype. *Proc Natl Acad Sci* 109(3):911–916
22. Jiang X, Bruzewicz DA, Wong AP, Piel M, Whitesides GM (2005) Directing cell migration with asymmetric micropatterns. *Proc Natl Acad Sci* 102(4):975–978
23. Brock A, Chang E, Ho C-C, LeDuc P, Jiang X, Whitesides GM, Ingber DE (2003) Geometric determinants of directional cell motility revealed using microcontact printing. *Langmuir* 19(5):1611–1617
24. Duffy DC, McDonald JC, Schueller OJA, Whitesides GM (1998) Rapid Prototyping of Microfluidic Systems in Poly(dimethylsiloxane). *Anal Chem* 70(23):4974–4984
25. Aratyn-Schaus Y, Oakes PW, Stricker J, Winter SP, Gardel ML (2010) Preparation of compliant matrices for quantifying cellular contraction. *J Vis Exp* 46:2173
26. Crocker JC, Grier DG (1996) Methods of digital video microscopy for colloidal studies. *J Colloid Interface Sci* 179(1):298–310
27. Sabass B, Gardel ML, Waterman CM, Schwarz US (2008) High Resolution Traction Force Microscopy Based on Experimental and Computational Advances. *Biophys J* 94(1):207–220
28. Edwards CM, Schwarz US (2011) Force localization in contracting cell layers. *Phys Rev Lett* 107(12):128101
29. Weijer CJ (2009) Collective cell migration in development. *J Cell Sci* 122(Pt 18):3215–3223
30. Rørth P (2009) Collective Cell Migration. *Annu Rev Cell Dev Biol* 25(1):407–429
31. Friedl P, Gilmour D (2009) Collective cell migration in morphogenesis, regeneration and cancer. *Nat Rev Mol Cell Biol* 10(7):445–457
32. Tambe DT, Hardin CC, Angelini TE, Rajendran K, Park CY, Serra-Picamal X, Zhou EH, Zaman MH, Butler JP, Weitz DA, Fredberg JJ, Trepats X (2011) Collective cell guidance by cooperative intercellular forces. *Nat Mater* 10(6):469–475
33. Kim JH, Serra-Picamal X, Tambe DT, Zhou EH, Park CY, Sadati M, Park J-A, Krishnan R, Gweon B, Millet E, Butler JP, Trepats X, Fredberg JJ (2013) Propulsion and navigation within the advancing monolayer sheet. *Nat Mater* 12(9):856–863
34. Straight AF, Cheung A, Limouze J, Chen I, Westwood NJ, Sellers JR, Mitchison TJ (2003) Dissecting temporal and spatial control of cytokinesis with a myosin II inhibitor. *Science* 299(5613):1743–1747
35. Uehata M, Ishizaki T, Satoh H, Ono T, Kawahara T, Morishita T, Tamakawa H, Yamagami K, Inui J, Maekawa M, Narumiya S (1997) Calcium sensitization of smooth muscle mediated by a Rho-associated protein kinase in hypertension. *Nature* 389(6654):990–994
36. Pelham RJ, Wang YL (1997) Cell locomotion and focal adhesions are regulated by substrate flexibility. *Proc Natl Acad Sci* 94(25):13661–13665
37. Butler JP, Tolić-Nørrelykke IM, Fabry B, Fredberg JJ (2002) Traction fields, moments, and strain energy that cells exert on their surroundings. *Am J Physiol Cell Physiol* 282(3):C595–C605
38. Berginski ME, Vitriol EA, Hahn KM, Gomez SM (2011) High-resolution quantification of focal adhesion spatiotemporal dynamics in living cells. *PLoS ONE* 6(7):e22025
39. Tojkander S, Gateva G, Lappalainen P (2012) Actin stress fibers - assembly, dynamics and biological roles. *J Cell Sci* 125(8):1855–1864
40. Bement WM, Mandato CA, Kirsch MN (1999) Wound-induced assembly and closure of an actomyosin purse string in *Xenopus* oocytes. *Curr Biol* 9(11):579–587
41. Martin P, Lewis J (1992) Actin cables and epidermal movement in embryonic wound healing. *Nature* 360(6400):179–183

doi:10.1186/1559-4106-8-32

Cite this article as: Rausch et al.: Polarizing cytoskeletal tension to induce leader cell formation during collective cell migration. *Biointerphases* 2013 **8**:32.

Submit your manuscript to a SpringerOpen® journal and benefit from:

- Convenient online submission
- Rigorous peer review
- Immediate publication on acceptance
- Open access: articles freely available online
- High visibility within the field
- Retaining the copyright to your article

Submit your next manuscript at ► springeropen.com